



# Incompressible Rayleigh–Taylor Turbulence

Guido Boffetta<sup>1,2</sup> and Andrea Mazzino<sup>3,4,5</sup>

<sup>1</sup>Department of Physics, University of Torino, Torino 10125, Italy;  
email: guido.boffetta@unito.it

<sup>2</sup>INFN, Section of Torino, Torino 10125, Italy

<sup>3</sup>Department of Civil, Chemical, and Environmental Engineering, University of Genova, Genova 16145, Italy; email: andrea.mazzino@unige.it

<sup>4</sup>CINFAI, Section of Genova, Genova 16145, Italy

<sup>5</sup>INFN, Section of Genova, Genova 16146, Italy

Annu. Rev. Fluid Mech. 2017. 49:119–43

The *Annual Review of Fluid Mechanics* is online at  
fluid.annualreviews.org

This article's doi:  
10.1146/annurev-fluid-010816-060111

Copyright © 2017 by Annual Reviews.  
All rights reserved

## Keywords

turbulent convection, mixing, heat and mass transfer, complex flows

## Abstract

Basic fluid equations are the main ingredient in the development of theories of Rayleigh–Taylor buoyancy-induced instability. Turbulence arises in the late stage of the instability evolution as a result of the proliferation of active scales of motion. Fluctuations are maintained by the unceasing conversion of potential energy into kinetic energy. Although the dynamics of turbulent fluctuations is ruled by the same equations controlling the Rayleigh–Taylor instability, here only phenomenological theories are currently available. The present review provides an overview of the most relevant (and often contrasting) theoretical approaches to Rayleigh–Taylor turbulence together with numerical and experimental evidence for their support. Although the focus is mainly on the classical Boussinesq Rayleigh–Taylor turbulence of miscible fluids, the review extends to other fluid systems with viscoelastic behavior, affected by rotation of the reference frame, and, finally, in the presence of reactions.

## 1. INTRODUCTION

Rayleigh–Taylor (RT) instability arises at the interface of two fluids of different densities in the presence of relative acceleration. RT instability and its late-stage evolution in a fully developed turbulent regime are ubiquitous spontaneous mixing phenomena occurring in many natural systems with unstably stratified interfaces. They also occur over a huge interval of spatial and temporal scales, ranging from everyday-life phenomena to astrophysical processes (see **Figure 1**).

In astrophysics, RT instability is thought to have profound consequences for flame acceleration in type Ia supernova. It is possible that this acceleration, operating on the stellar scale, can bring the flame speed up to a significant fraction of the speed of sound, which has important consequences in modeling type Ia supernovae (see, e.g. Hillebrandt & Niemeyer 2000, Bell et al. 2004). In geology, multiwavelength RT instability has been invoked to explain the initiation and evolution of polydiapirs (domes in domes) (see, e.g., Weinberg & Schmeling 1992). Moreover, the possibility that intraplate orogeny is the result of RT instability in the Earth’s mantle lithosphere beneath the orogenic zone has been explored by means of a two-layered model (Neil & Houseman 1999). In atmospheric fluid dynamics and cloud physics, RT instability has been invoked by Agee (1975) to try to solve the intriguing enigma related to the formation of the fascinating mammatus clouds. As discussed by Shultz et al. (2006), the situation is, however, still rather controversial and further investigations are needed.

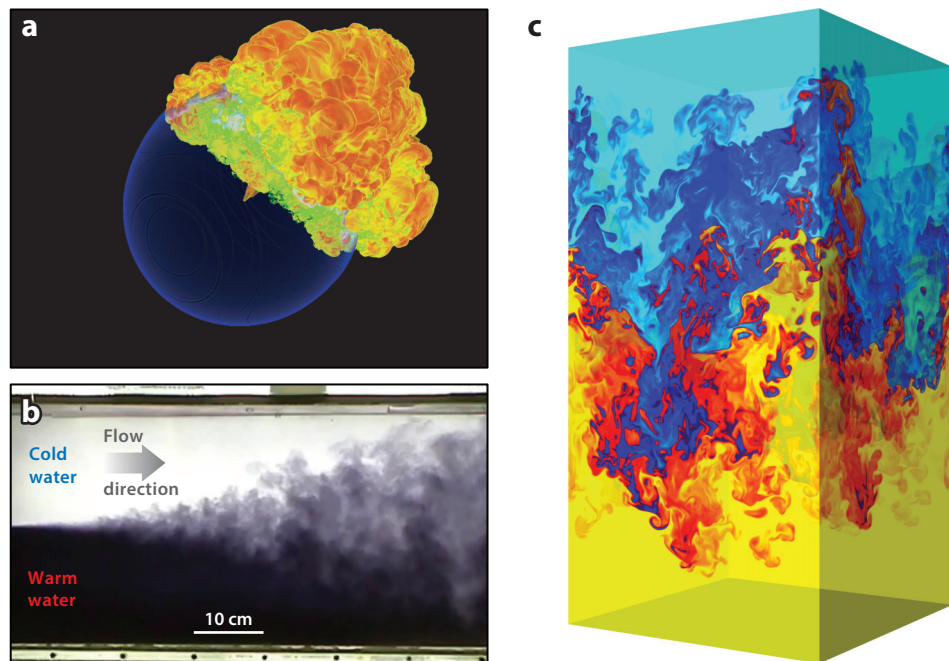


**Figure 1**

(a) Thermonuclear flame plume bursting through the surface of a white dwarf during a supernova explosion. Panel *a* provided by the Flash Center for Computational Science, University of Chicago. (b) Rayleigh–Taylor mixing experiment in a water channel. The upper, clear, heavy water mixes by Rayleigh–Taylor instability with lower, dark, light water, generating turbulent mixing. Panel *b* courtesy of A. Banerjee. (c) Color representation of the temperature field  $T(\mathbf{x})$  (with *yellow* representing hot, and *blue* cold) from a direct numerical simulation of the Boussinesq equations (Equations 2–3) in the late stage of Rayleigh–Taylor turbulence.

RT instability and turbulence also have key roles in several technological applications, such as inertial confinement fusion and disruption of radio-wave propagation within the terrestrial ionosphere. In inertial confinement fusion, the RT instability causes premature fuel mixing (due to beam-beam imbalance or beam anisotropy), thus reducing heating efficacy at the time of maximum compression (see, e.g., Kilkenny et al. 1994, Tabak et al. 1994). In the terrestrial ionosphere, electromagnetic waves are scattered because of irregularities in plasma density. RT instability is invoked to explain these irregularities (see, e.g., Sultan 1996).

Even if, in all discussed cases, the basic mechanism of RT instability and turbulence is a buoyancy-induced fluid-mixing mechanism, many other ingredients may actually come into play. These include surface tension and viscosity (see, e.g., Bellman & Pennington 1954, Mikaelian 1993, Chertkov et al. 2005, Celani et al. 2009, Boffetta et al. 2010c), magnetic fields (Kruskal & Schwarzschild 1954, Peterson et al. 1996), spherical geometries (Plesset 1954, Sakagami & Nishihara 1990), finite-amplitude perturbations (Chang 1959), bubbles (Garabedian 1957, Hecht et al. 1994, Goncharov 2002), rotation (Chandrasekhar 1961, Baldwin et al. 2015), and compressibility (Newcomb 1983, Livescu 2004, 2013, Scagliarini et al. 2010).

The field of RT instability appears to be very mature, and there already exist excellent reviews of parts of the instability theory, especially those by Chandrasekhar (1961) and more recently by Sharp (1984) and Abarzhi (2010b). Chandrasekhar (1961) provided an overview of the linear theory for incompressible continuous media, whereas Sharp (1984) also surveyed nonlinear phenomenological models. Abarzhi (2010b) extended the review to the nonlinear mixing stage. The textbook by Drazin & Reid (1981) represents another valuable introduction to hydrodynamic instabilities. Thermal instabilities and shear flow instabilities are the main concern of the excellent review by Kull (1991). Andrews & Dalziel (2010) reported recent progress in experiments on RT mixing at low Atwood numbers (see also the sidebar, Rayleigh–Taylor Experiments).

Our aim here is to summarize approximately one decade of research activity on the phenomenology of (miscible) Boussinesq RT turbulence after the seminal paper of Chertkov (2003). This paper deeply changed the general understanding of Boussinesq RT turbulence: It now appears as a classical hydrodynamical turbulence system in which the role of gravity is simply to act as a time-dependent pumping scale. Familiar concepts borrowed from the classical theory, à la Kolmogorov, of turbulent flows have thus been exploited for the Boussinesq RT system with many predictions for relevant statistical observables. These predictions triggered new studies with the final aim of confirming or contradicting the new theory. One of the main aims of our review is to summarize the current state of the art in this respect. Moreover, we provide a guided tour of generalizations of classical Boussinesq RT turbulence, including viscoelastic RT turbulence and RT mixing under rotation, with the hope that they could trigger new experimental activities in this field, as well as make interesting comparisons and connections with the Rayleigh–Bénard (RB) turbulent system. Given space constraints, we do not review many interesting and important aspects of RT mixing dealing with non-Boussinesq effects, immiscibility, compressibility, and complex geometry.

## 2. OBERBECK–BOUSSINESQ EQUATIONS FOR RAYLEIGH–TAYLOR TURBULENCE

One important application of RT instability is the case of convective flow, in which density differences reflect temperature fluctuations of a single fluid and the acceleration is provided by gravity, which is uniform in space. The problem is further simplified within the so-called Oberbeck–Boussinesq (OB) approximation (see, e.g., Tritton 1988), which assumes incompressible flows and small variations of the density. In this limit, the density  $\rho$  linearly depends on the temperature  $T$

## RAYLEIGH–TAYLOR EXPERIMENTS

In contrast with RB convection, there is not a standard setup for RT turbulence, and several experiments have been proposed to generate the initial state, which is, by definition, unstable. Different techniques have been developed to stabilize the initial configuration, starting from compressed gas experiments by Lewis (1950) in a thin layer. In the Rocket-Rig apparatus of Read (1984) (see also Youngs 1992), the initial stable configuration (light fluid over heavy fluid) is accelerated downward by a small rocket motor with an acceleration larger than gravity. The evolution of the instability is limited in time (by the vertical extension of the setup), and this required the use of large Atwood numbers or immiscible fluids (Andrews & Dalziel 2010). A more recent variant of this setup, developed by Dimonte & Schneider (1996), uses a linear electric motor, which allows control of the acceleration profile.

The overturning tank developed by Andrews & Spalding (1990) generates the instability by rotating a narrow tank mounted on a horizontal axis. This setup overcomes the problem of the small-Atwood number experiments of the Rocket-Rig apparatus, and working fluids are typically freshwater and brine solution with  $A \simeq 0.05$ . The sliding barrier experiment developed by Linden et al. (1994) uses a removable metal sheet to separate the two layers of fluid at different densities (again brine and freshwater). One problem with this setup is the generation of viscous boundary layers around the sheet when it is removed. The setup was later improved by Dalziel (1993), who used nylon fabric wrapped around the metal plate to eliminate the boundary layers. A similar setup, developed by Rivera & Ecke (2007), uses a stretched latex membrane to separate the two layers. When the latex membrane is ruptured with a needle, the instability starts. This setup was used to investigate RT mixing at  $A \simeq 0.003$  and small aspect ratio (lateral dimensions one-fifth the vertical size), and the growth of the mixing layer was found to be slower than  $t^2$ .

A different setup, developed by Snider & Andrews (1994), uses a water channel in which two water streams at different densities (temperatures) flow parallel separated by a thin horizontal plate. At the end of the plate, the streams enter the test channel, where they meet and the RT instability develops. The main advantage of the present setup is that mixing evolves in space and not in time, allowing for time averages over a statistically stationary state. The original channel was developed for very small Atwood numbers ( $A \sim 10^{-3}$ ), whereas a more recent setup developed by Banerjee & Andrews (2006) is capable of reaching  $A \simeq 1$ . Another promising technique developed by Huang et al. (2007) makes use of a strong magnetic field gradient to stabilize a paramagnetic (heavy) fluid over a diamagnetic (light) one. In yet another variant, the initial configuration is opposite (and stable), and the magnetic field is used to produce the instability (Baldwin et al. 2015).

as

$$\rho(T) = \rho(T_0) [1 - \beta(T - T_0)], \quad (1)$$

where  $T_0$  is a reference temperature, and the thermal expansion coefficient  $\beta$  (as well as the viscosity  $\nu$  and the thermal diffusivity  $\kappa$ ) is assumed constant, independent of  $T$ . The OB equations of motion for the velocity  $\mathbf{u}(\mathbf{x}, t)$  and temperature  $T(\mathbf{x}, t)$  in the gravitational field  $\mathbf{g} = (0, 0, -g)$  are

$$\partial_t \mathbf{u} + \mathbf{u} \cdot \nabla \mathbf{u} = -\nabla p + \nu \nabla^2 \mathbf{u} - \beta \mathbf{g} T, \quad (2)$$

$$\partial_t T + \mathbf{u} \cdot \nabla T = \kappa \nabla^2 T, \quad (3)$$

together with the incompressibility condition  $\nabla \cdot \mathbf{u} = 0$  ( $p$  represents the pressure field). Under the OB approximation, the fluid motion is symmetric for vertical reflection: Indeed, Equations 2 and 3 are invariant for  $\mathbf{g} \rightarrow -\mathbf{g}$  and  $T \rightarrow -T$ . The RT configuration is defined by the initial condition of unstable stratification with a horizontal interface (generally normal to the

acceleration) that separates a layer of cooler (heavier, of density  $\rho_2$ ) fluid from a lower layer of hotter (lighter, of density  $\rho_1$ ) fluid, both at rest [i.e.,  $T(\mathbf{x}, 0) = -(\theta_0/2)\text{sgn}(z)$  and  $\mathbf{u}(\mathbf{x}, 0) = 0$ ].  $\theta_0$  is the temperature jump across the layers (symmetric with respect to  $T_0$ ) that fixes the Atwood number  $A = (\rho_2 - \rho_1)/(\rho_2 + \rho_1) = \beta\theta_0/2$ . Although the Atwood number must be small for the OB limit to be valid, when working within this approximation  $A$  simply rescales the effect of gravity on the buoyancy force and thus the characteristic time of the phenomena. Below we always assume the validity of the OB approximation; therefore, we use either a density fluctuation or temperature fluctuation as the two are related by Equation 1.

The RT configuration is unstable to perturbations of the interface. For a single-mode perturbation of wave number  $k$ , linear stability analysis for an inviscid potential flow gives the growth rate of the amplitude as (see Lamb 1932; reviewed in Kull 1991)

$$\lambda = \sqrt{Agk}. \quad (4)$$

According to Equation 4, the growth rate increases indefinitely with  $k$ , thus favoring the growth of short-wavelength perturbations. Several physical effects can limit the growth at large wave numbers, including surface tension, viscosity (Chandrasekhar 1961, Menikoff et al. 1977), and diffusivity (Duff et al. 1962). Linear stability analysis has been also generalized to include other physical ingredients, including rotation (Chandrasekhar 1961), compressibility (Mitchner & Landshoff 1964), viscoelasticity (Boffetta et al. 2010b), and nonuniform acceleration (Kull 1991).

### 3. PHENOMENOLOGY OF RAYLEIGH-TAYLOR TURBULENCE

The linear phase of the instability, discussed in Section 2, breaks down when the amplitude of the perturbation of the interface becomes comparable with the wavelength. At this point, nonlinear effects emerge and the RT flow develops into a different, nonlinear phase. This nonlinear phase is characterized by the formation of ascending and descending plumes that detach from the original region of hot or cold fluid and enter the opposite region, thus enhancing the heat transport between the two reservoirs. At this point, the interface between the two regions is no longer single valued, and several modes are activated, eventually leading to the turbulent phase.

The phenomenology of the temporal evolution of the turbulent phase can be derived dimensionally starting from the energy equation. Introducing the kinetic energy density  $E = (1/2)\langle|\mathbf{u}|^2\rangle$  (where  $\langle\cdots\rangle$  indicates average over the space), from Equation 2, one obtains

$$\frac{dE}{dt} = \beta g \langle wT \rangle - \varepsilon_v = -\frac{dP}{dt} - \varepsilon_v, \quad (5)$$

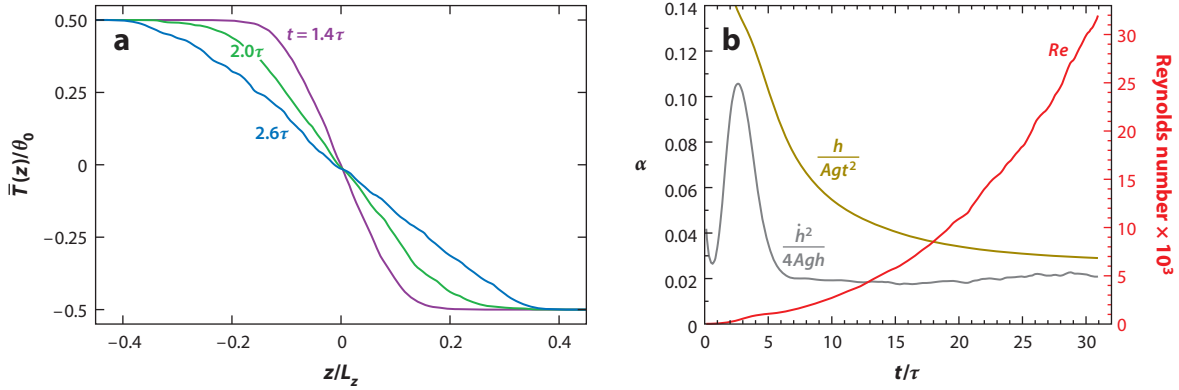
where we have introduced the potential energy of the system,  $P \equiv -\beta g \langle zT \rangle$ , and the viscous energy dissipation rate,  $\varepsilon_v = \nu \langle (\nabla \mathbf{u})^2 \rangle$ . For simplicity, in Equation 5 we neglect the contribution of thermal diffusivity as it is smaller than the other terms. By introducing the typical velocity fluctuation  $U$  (defined, e.g., as the root mean square of the vertical component  $w$ ), one has dimensionally from Equation 5

$$\frac{dU^2}{dt} \simeq \beta g U \theta_0, \quad (6)$$

because the temperature fluctuation at the integral scale is  $\theta_0$  and therefore, by integration,

$$U(t) \simeq Agt; \quad (7)$$

i.e., the large-scale velocity fluctuation grows linearly in time. Given that this is the velocity that moves the plumes within the mixing layer, by integration, one obtains the dimensional prediction


**Figure 2**

(a) Mean temperature profile  $\bar{T}(z, t)$  from a numerical simulation of Rayleigh–Taylor turbulence [ $\tau = (L_z/Ag)^{1/2}$ ]. Panel a adapted with permission from Boffetta et al. (2009). (b) Evolution of the mixing layer thickness  $h(t)$  and its growth rate  $\dot{h}(t)$  normalized by the Atwood number  $A$ , gravity  $g$ , and time, as a function of time. Panel b adapted with permission from Cabot & Cook (2006).

for the quadratic growth of the layer width  $h(t)$ :

$$h(t) = \alpha Ag t^2, \quad (8)$$

where the dimensionless parameter  $\alpha$  represents the efficiency of the conversion of potential energy into kinetic energy. The phenomenology of small-scale RT turbulence, discussed in Section 4, assumes that within the mixing layer a turbulent cascade à la Kolmogorov develops, with an integral scale  $h$  that grows in time according to Equation 8 and an energy flux given dimensionally by  $\varepsilon \simeq U^3/h \simeq (Ag)^2 t$ .

**Figure 2** shows the mean temperature profile  $\bar{T}(z, t)$  as a function of  $z$  at different times. The profile is obtained by averaging the temperature field shown in **Figure 1** over the horizontal plane  $(x, y)$  and over different realizations of the numerical simulations. From this plot, it is evident that the inner region of the mixing layer develops a linear temperature profile  $\bar{T}(z, t) \simeq -\gamma(t)z$  with a gradient that dimensionally decreases as  $\gamma(t) \simeq \theta_0/h \simeq t^{-2}$  [see Boffetta et al. 2009 for the three-dimensional (3D) case and Celani et al. 2006, Biferale et al. 2010, and Zhou 2013 in two dimensions]. Different definitions of the width of the mixing layer have been proposed, based on either local or global properties of  $\bar{T}(z)$ . The simplest measure is based on the threshold value  $b_r$  at which  $\bar{T}(z)$  reaches a fraction  $r$  of the maximum value [i.e.,  $\bar{T}(\pm b_r/2) = \mp r\theta_0/2$ ] (see, e.g., Dalziel et al. 1999). Other definitions, proposed by Cabot & Cook (2006) and Vladimirova & Chertkov (2009), are based on integral quantities, i.e.,  $b_M = \int M(\bar{T})dz$ , where  $M$  is an appropriate mixing function that has support on the mixing layer only. The linearity of the mean temperature profile implies statistical homogeneity inside the mixing layer, a key ingredient for the development of a phenomenological theory of turbulent fluctuations based on Kolmogorov (1941) (see Section 4). Deviations from this linear profile, with the crossover of  $\bar{T}(z)$  to the bulk values  $\pm\theta_0/2$ , can indeed be understood as a manifestation of the nonhomogeneity of turbulence at the edge of the mixing layer. These deviations can be captured by a mixing length model with  $z$ -dependent eddy diffusivity, as shown by Boffetta et al. (2010a) and Biferale et al. (2011b).

### 3.1. Models for the Evolution of the Mixing Layer

Fermi & von Neumann (1955) were among the first to address the nonlinear evolution of the interface. In their unpublished note, they assumed a rectangular plume that moves vertically, pushed by gravity. In the simplified version of up-down symmetry (Boussinesq approximation), the variation of the potential energy given by a couple of plumes (of densities  $\rho_1$  and  $\rho_2$ ) of square base  $b^2$  and height  $b$  moving in the region of different density is

$$\Delta P = (\rho_1 - \rho_2)b^2 gb^2, \quad (9)$$

which is negative as the potential energy decreases. If the plumes are moving with constant vertical velocity  $\dot{b}$ , the change in the kinetic energy in the system is

$$\Delta E = \frac{1}{2}(\rho_1 + \rho_2)b^2 hb\dot{b}. \quad (10)$$

By using the Euler–Lagrange equation  $\partial L/\partial b = d/dt(\partial L/\partial \dot{b})$  for the Lagrangian  $L = E - 2\alpha P$ , one obtains

$$\ddot{b}b + \frac{1}{2}\dot{b}^2 = 4\alpha Agb, \quad (11)$$

where  $\alpha$  is the same parameter as in Equation 8, here representing (with a factor of two) the fraction of the potential energy converted into the kinetic energy of the plumes (while the fraction  $1 - 2\alpha$  is dissipated by viscosity and diffusivity). The solution to Equation 11 for the initial height  $b(0) = b_0$  is given by

$$b(t) = b_0 + 2(\alpha Agb_0)^{1/2}t + \alpha Agt^2. \quad (12)$$

When extended from a single plume to the whole interface, this solution shows that asymptotically the growth of the mixing layer follows the well-known accelerated law  $b(t) = \alpha Agt^2$ , but this regime dominates after a transient that lasts up to a time  $\propto (b_0/(\alpha Ag))^{1/2}$ .

Recently, the Fermi & von Neumann (1955) result (Equation 11) has been rediscovered by different authors and using different arguments. Ristorcelli & Clark (2004) used a self-similar analysis of the Navier–Stokes equations, whereas Cook et al. (2004) used a mass flux and energy balance argument. Both obtain the same equation for the growth of the mixing width  $b$ :

$$\dot{b}^2 = 4\alpha Agb, \quad (13)$$

which is a particular case of Equation 11 and admits the same solution (Equation 12).

One useful application of this approach is for data analysis in order to measure the dimensionless coefficient  $\alpha$ . The determination of  $\alpha$  and its possible universality have indeed been the object of many studies. The picture that emerges is that the measurement of  $\alpha$  from the fit of  $b(t)$  with  $t^2$  is sensitive to the transient behavior, which depends on the initial perturbation of the interface. In general, experimental measurements give a value of  $\alpha$  in the range 0.05–0.07 (Read 1984, Linden et al. 1994, Snider & Andrews 1994, Dimonte & Schneider 1996, Schneider et al. 1998, Banerjee & Andrews 2006), whereas numerical simulations report lower values, around 0.03 (Youngs 1991, Young et al. 2001, Dimonte et al. 2004, Cabot & Cook 2006, Vladimirova & Chertkov 2009). One possible origin of this difference is the presence of long-wavelength perturbations in the experiments, whereas numerical simulations are usually perturbed at small scales (Ramaprabhu & Andrews 2004, Banerjee & Andrews 2009, Wei & Livescu 2012). Indeed, when these long-wavelength perturbations are present in the initialization of the simulations, the results are closer to those from experiments. The basic idea of this approach is to directly use Equation 13, i.e., to measure  $\alpha$  as  $\alpha = \dot{b}^2/(4Agb)$  instead of  $\alpha = b/(Agt^2)$  (Ristorcelli & Clark 2004). **Figure 2** compares the two methods, showing that the similarity method converges to a constant value of  $\alpha$  much faster than the standard method. The slow convergence of  $b/(Agt^2)$  (resulting from

the presence of the constant and linear terms in Equation 12) is probably one of the reasons why different simulations, characterized by different Reynolds numbers (i.e., resolutions), give different results for the value of  $\alpha$ .

### 3.2. Global Heat Transfer Scaling

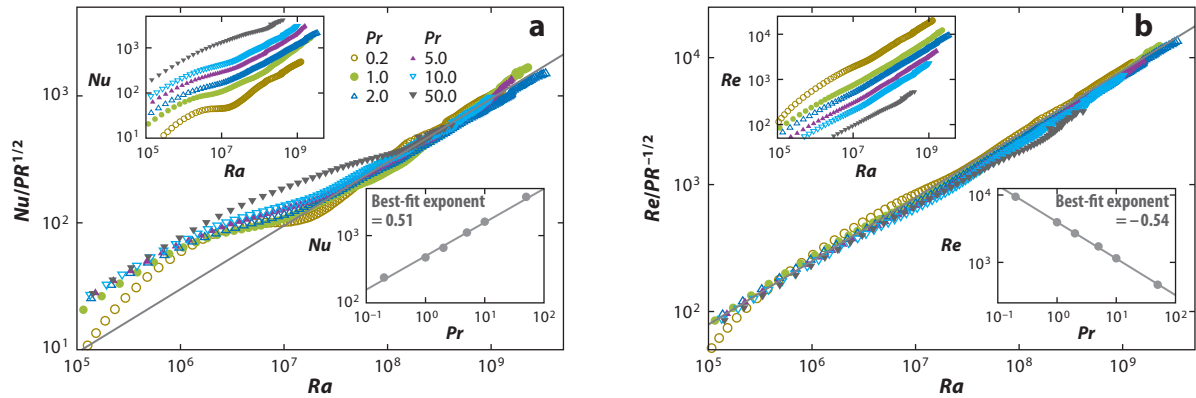
RT turbulence represents an example of turbulent thermal convection in which heat is transferred, thanks to the work done by buoyancy forces, between the cold (heavy) and hot (light) portions of fluid. Heat transfer in RT turbulence is inherently associated with the presence of turbulence, as the turbulent layer, during its growth, penetrates and mixes the two reservoirs of fluids at different temperatures. In this sense, thermal transfer in RT turbulence is quite different from the phenomenology observed in RB turbulence, probably the most studied prototype of turbulent convection (e.g., reviewed in Siggia 1994, Bodenschatz et al. 2000, Lohse & Xia 2010). We recall that the heat transfer in RB convection is dominated by the physics at the boundary layers (both thermal and kinetic), which develop in correspondence with the two plates. Those boundary layers, together with the large-scale convective motion, are responsible for the heat transfer between the two plates, and different regimes have been identified according to the dominant contribution (thermal or kinetic boundary layer or bulk) (Grossmann & Lohse 2000, Ahlers et al. 2009).

In general, the dimensionless measure of the heat transfer efficiency is given by the Nusselt number  $Nu$ , defined as the ratio of the global turbulent heat transfer to the molecular one, whereas turbulence intensity is measured, as usual, by the Reynolds number  $Re$ . These two numbers depend on the control parameters, which are the Rayleigh number  $Ra$  (a dimensionless measure of the temperature difference that forces the system) and the Prandtl number  $Pr = \nu/\kappa$ . A basic problem in thermal convection is the characterization of the state of the system as a function of the parameters, i.e., the functional relations  $Nu(Ra, Pr)$  and  $Re(Ra, Pr)$ . Many experimental (Niemela et al. 2000, Funfschilling et al. 2009) and numerical (Stevens et al. 2010) studies, supported by theoretical arguments (Siggia 1994, Grossmann & Lohse 2000, Ahlers et al. 2009), show that, for Rayleigh numbers much larger than the critical number for the onset of convection, a scaling regime develops under which

$$Nu \simeq Ra^\gamma Pr^\delta, \quad Re \simeq Ra^{\gamma'} Pr^{\delta'}. \quad (14)$$

Several theories have been proposed to predict the values of the scaling exponents in Equation 14 in RB convection (reviewed in Siggia 1994; Ahlers et al. 2009). Briefly, we mention that recent experimental and numerical data, characterized by a wide extension in the parameter space and high precision, show that the heat transfer in RB convection probably cannot be captured by simple scaling laws, and this phase diagram in the  $(Ra, Pr)$  space is more complex than expected (Grossmann & Lohse 2000, Ahlers et al. 2009).

One fixed point in the space of the theories on turbulent convection is that, for large-enough Rayleigh numbers, the effects of boundary layers disappear, and a transition to a new regime dominated by bulk contributions occurs. This regime, first predicted by Kraichnan (1962) and later discussed by Spiegel (1971), is known as the ultimate state of thermal convection and is characterized by the simple set of scaling exponents  $\gamma = \delta = \gamma' = 1/2$ ,  $\delta' = -1/2$ . Despite the large body of experimental and numerical efforts, the ultimate regime remained elusive in RB convection, even at the largest  $Ra$  achieved. On the contrary, it has been observed both in numerical simulations of convection in the absence of boundaries (Lohse & Toschi 2003) and in laboratory experiments in convective cells with elongated geometries that reduce the effects of the upper and lower walls (Gibert et al. 2006, Cholemani & Arakeri 2009).


**Figure 3**

(a) Nusselt number ( $Nu$ ) and (b) Reynolds number ( $Re$ ) as a function of Rayleigh number ( $Ra$ ) from a set of direct numerical simulations of Rayleigh–Taylor turbulence at different Prandtl numbers. The gray line in the main plot represents  $Ra^{1/2}$  scaling. (Upper insets, a)  $Nu$  and (b)  $Re$  without the  $Pr$  compensation. (Lower insets, a)  $Nu$  and (b)  $Re$  versus  $Pr$  at fixed  $Ra = 3 \times 10^8$ . The gray lines in the insets represent the best-fit exponents (a) 0.51 and (b)  $-0.54$ . Figure adapted with permission from Boffetta et al. (2012b).

The above discussion suggests that RT turbulence is a good candidate to observe the ultimate regime. No boundary layers are indeed present in the RT system. The ultimate state scaling emerges from the energy balance (Equation 5). The appropriate definition of the Rayleigh number is in terms of the mixing layer height  $h$  as  $Ra \equiv \beta g \theta_0 h^3 / (\nu \kappa)$ , whereas the Reynolds and Nusselt numbers are, respectively,  $Re \equiv Ub/\nu$  ( $U$  is a typical large-scale velocity) and  $Nu = \langle wT \rangle h / (\kappa \theta_0)$ . We can rewrite Equation 5 as

$$\kappa \frac{\beta g \theta_0}{h} Nu = \frac{d}{dt} \frac{1}{2} \langle u^2 \rangle + \varepsilon_\nu. \quad (15)$$

By using the dimensional behavior (Equations 7 and 8) for  $b(t)$  and  $U(t)$ , we obtain the temporal behavior  $Nu \simeq (\beta g \theta_0)^2 t^3 / \kappa$ . From the above definition of the Rayleigh number, we have  $Ra \simeq (\beta g \theta_0)^4 t^6 / (\nu \kappa)$  and therefore

$$Nu \simeq Ra^{1/2} Pr^{1/2}. \quad (16)$$

Similarly, from the definition of the Reynolds number, we have  $Re \simeq (\beta g \theta_0)^2 t^3 / \nu$  and thus

$$Re \simeq Ra^{1/2} Pr^{-1/2}. \quad (17)$$

The energy balance leading to Equation 15 is independent of the dimensionality; therefore, the ultimate state regime is also expected to hold in 2D RT turbulence even though, in this case, the energy flows to large scales (and hence  $\varepsilon_\nu = 0$ ), generating a different spectrum (see Section 4).

**Figure 3** shows the functional dependence of  $Nu(Ra, Pr)$  and  $Re(Ra, Pr)$  obtained from direct numerical simulations (DNS) of RT turbulence at high resolution. Several simulations, characterized by different  $Pr$ , have been performed starting from the same initial condition. Numerical data for the Nusselt number  $Nu$  are compatible with the scaling (Equation 16) for  $Ra > 10^7$  and for  $0.2 \leq Pr \leq 10$ . Some statistical fluctuations are observed, in particular for high  $Pr$ . The lower insets in **Figure 3** show the dependence on  $Pr$  obtained by computing  $Nu$  at fixed  $Ra$ . The best fit gives a slope  $0.51 \pm 0.02$ , compatible with Equation 16. The analysis for the Reynolds number shows a similar result, marginally compatible with Equation 17 for  $Ra > 10^6$ . In contrast with  $Nu$ , here the dependence on  $Pr$  gives a best-fit slope ( $-0.54 \pm 0.01$ ) that deviates from the theoretical prediction. The origin of this small deviation is unknown, but it could be from finite size effects that affect the definition of integral quantities.

#### 4. TWO-POINT STATISTICAL OBSERVABLES

Two-point statistical observables, which involve averaged field differences between a couple of points, are key observables in turbulence (see, e.g., Frisch 1995, Sreenivasan & Antonia 1997) as they are linked to experimentally measurable scale-dependent quantities, such as the kinetic energy spectrum or potential energy spectrum in gravity-driven flows. A long-standing challenge in RT turbulence is to determine universal scaling laws for inertial range two-point statistics, as done by Kolmogorov (1941) in ideal hydrodynamics turbulence.

Different theories for turbulent fluctuations have been proposed for RT turbulence. Chertkov (2003) analyzed the advanced mixing regime of RT turbulence in the small-Atwood number Boussinesq approximation. A Kolmogorov–Obukhov (K41) scenario for velocity and temperature spectra is predicted in three dimensions, whereas a Bolgiano–Obukhov (BO59) scenario is shown to arise in two dimensions. Mikaelian (1989) derived the turbulent energy and its spectrum in the Canuto–Goldman model (Canuto & Goldman 1985) when the turbulence is generated by an instability having a power-law growth rate. This model does not predict a Kolmogorov spectrum. For quantitative results in this respect, readers are referred to Soulard et al. (2015).

Zhou (2001) proposed a modification of the classical Kolmogorov framework by substituting the timescale for the decay of transfer function correlations, resulting from nonlinear interactions, with the typical timescale arising from the linear theory of RT instability,  $(kgA)^{-1/2}$ . A non-Kolmogorov scaling,  $k^{-7/4}$ , emerges for the energy spectrum. The insertion of a linear timescale in a fully developed turbulent regime seems, however, not fully justified. On the basis of symmetries of turbulent dynamics, Abarzhi (2010a) analyzed the influence of momentum transport on the properties of the turbulent RT system. The resulting scaling law is  $k^{-2}$  and thus distinct from Kolmogorov scaling. A similar spectrum was proposed within the momentum model of Sreenivasan & Abarzhi (2013). Soulard & Griffond (2012) calculated the anisotropic correction to the isotropic inertial range Kolmogorov scaling in terms of a perturbative approach. This approach is justified on the basis of numerical evidence from Boffetta et al. (2009) for 3D RT turbulence showing that, at small scales, the contribution of buoyancy forces to the energy flux becomes much smaller than the contribution of inertial nonlinear forces. Their results do not contradict the theory by Chertkov (2003). Moreover, Soulard (2012) adapted the Monin–Yaglom relation to RT turbulence both in three dimensions, which confirms the Kolmogorov–Obukhov theory, and in two dimensions, where it recovers the Bolgiano–Obukhov scenario proposed by Chertkov (2003). Finally, Poujade (2006) proposed a theory, based on a spectral equation, showing that a balance mechanism between buoyancy and spectral energy transfer can settle at low wave numbers in the self-similar regime. The above balance constrained the velocity spectrum in a way that was incompatible with the Kolmogorov–Obukhov mechanism. However, the theory does not rule out a Kolmogorov–Obukhov scenario at intermediate wave numbers. This proliferation of theoretical models, all reasonable and plausible, is ascribed to the variety of dynamical regimes in RT turbulence mainly due to the nonstationarity of the process.

The phenomenological theory by Chertkov (2003) considers a mixing layer in the self-similar regime with an integral scale  $b(t)$  and large-scale velocity  $U(t)$  given by Equations 8 and 7, respectively. Starting from these assumptions, for the 3D case Chertkov (2003) proposed a quasi-stationary, adiabatic generalization of the Kolmogorov–Obukhov picture of steady Navier–Stokes turbulence (Kolmogorov 1941, Obukhov 1941). The first step is to assume the existence of an inertial range of scales characterized by a scale-independent kinetic energy flux,  $\varepsilon(t)$ , given by the usual K41 relation:

$$\varepsilon(t) = \frac{U(t)^3}{b(t)} \simeq (\beta g \theta_0)^2 t, \quad (18)$$

where we neglect the coefficient  $\alpha = O(1)$ . Because of the explicit time dependence, the assumption of scale independence is justified only if the variation of the flux, a large-scale quantity, is slow to allow small-scale fluctuations to adjust adiabatically to the current value of the flux (Chertkov 2003). If  $\varepsilon$  is scale independent, following the standard Kolmogorov argument, one can write  $\varepsilon \simeq (\delta_r u^3)/r$ , where  $\delta_r u$  is the velocity fluctuation on a scale  $r$  belonging to the inertial range  $\eta(t) \ll r \ll b(t)$  and  $\eta$  is analogous to the Kolmogorov viscous scale, to be determined in the following. By standard power counting and exploiting Equation 18, one obtains

$$\delta_r u(t) \simeq (\beta g \theta_0)^{2/3} r^{1/3} t^{1/3}. \quad (19)$$

The same adiabatic idea extended to temperature fluctuations,  $\delta_r T$ —which should, similar to velocity fluctuations, cascade toward increasingly smaller scales at a constant rate—leads to the generalization of the Obukhov–Corrsin theory (OC51) of passive scalar advection (Obukhov 1949, Corrsin 1951),

$$\epsilon_T(t) \simeq \frac{\theta_0^2 U}{b} \simeq \frac{\delta_r T^2 \delta_r u}{r}, \quad (20)$$

valid in the same range of scales of Equation 19. Exploiting Equation 19, one sees that the scaling prediction for  $\delta_r T$  follows from Equation 20:

$$\delta_r T(t) \simeq \theta_0 (\beta g \theta_0)^{-1/3} r^{1/3} t^{-2/3}. \quad (21)$$

By simple power counting, it is easy to show from Equations 19 and 21 that temperature fluctuations are passively transported by the velocity field within the inertial range of scales [i.e.,  $\varepsilon(t) \gg \beta g \delta_r T \delta_r u$ ], in accord with the assumption that buoyancy acts only on scales around the integral scale  $b(t)$ .

The Kolmogorov (viscous) scale  $\eta(t)$  is defined as the scale below which the kinetic energy coming from the inertial range is dissipated by viscosity. It is defined by the balance  $\delta_\eta u^3/\eta \simeq \nu \delta_\eta u^2/\eta^2$ , from which, extending the validity of Equation 19 down to  $r = \eta$ , one has

$$\eta(t) \simeq \nu^{3/4} t^{-1/4} (\beta g \theta_0)^{-1/2}. \quad (22)$$

This time behavior has been verified via 3D DNS by Ristorcelli & Clark (2004). From Equation 22, the viscous Kolmogorov timescale  $\tau_\eta \equiv \eta/\delta_\eta u$  is

$$\tau_\eta \simeq (\beta g \theta_0)^{-1} \nu^{1/2} t^{-1/2}. \quad (23)$$

Note that  $b(t)/\eta(t)$  increases in time as  $t^{9/4}$ .

2D turbulence is characterized by two inviscid conserved quantities: kinetic energy and enstrophy. On the basis of standard arguments valid in 2D hydrodynamic turbulence (Boffetta & Ecke 2012), a double-cascade scenario sets in with energy flowing toward large scales (with respect to the pumping scale) and enstrophy going to small scales. This scenario is not compatible with the argument developed for three dimensions as the assumption  $\varepsilon(t) \gg \beta g \delta_r T \delta_r u$  is violated at large scales.

Chertkov (2003) proposed a new scenario in which buoyancy and velocity fluctuations balance scale by scale. This is the essence of the Bolgiano–Obukhov scenario introduced in the context of Rayleigh–Bénard convection (Bolgiano 1959, Obukhov 1959, Siggia 1994, Lohse & Xia 2010). In this case, the temperature is active at all scales, and the resulting scaling laws emerge by balancing

$$\frac{\delta_r u^2}{r} \simeq \beta g \delta_r T, \quad (24)$$

with temperature fluctuations cascading toward small scales at a constant rate according to Equation 20. Combining Equations 20 and 24, one obtains the Bolgiano scaling laws for both

velocity and temperature fluctuations:

$$\delta_r u \simeq (\beta g \theta_0)^{2/5} r^{3/5} t^{-1/5}, \quad (25)$$

$$\delta_r T \simeq \theta_0 (\beta g \theta_0)^{-1/5} r^{1/5} t^{-2/5}, \quad (26)$$

together with the prediction for the viscous scale  $\eta(t)$  and its associated timescale  $\tau_\eta \equiv \eta/\delta_\eta u$ :

$$\eta(t) \simeq (\beta g \theta_0)^{-1/4} \nu^{5/8} t^{1/8}, \quad \tau_\eta \simeq (\beta g \theta_0)^{-1/2} \nu^{1/4} t^{1/4}, \quad (27)$$

valid for  $\nu \gg \kappa$ . The ratio between the integral scale  $b(t)$  and viscous scale  $\eta(t)$  now increases as  $t^{15/8}$ , slower than in three dimensions.

#### 4.1. Spatial and Temporal Scaling Laws of Structure Functions and Spectra

The scaling relationships in Equations 19 and 21, in three dimensions, and Equations 25 and 26, in two dimensions, set the dimensional predictions for both velocity and temperature fluctuations in the spatial and temporal domains. Neglecting possible intermittency fluctuations, these predictions can be used to build (dimensional) scaling laws of structure functions and isotropic spectra. For the 3D case, velocity and temperature structure functions and spectra are

$$S_p(r) = \left\langle \left[ (\mathbf{u}(\mathbf{r}, t) - \mathbf{u}(\mathbf{0}, t)) \cdot \frac{\mathbf{r}}{r} \right]^p \right\rangle \simeq (\beta g \theta_0)^{2p/3} t^{p/3} r^{p/3}, \quad (28)$$

$$E(k) \simeq (\beta g \theta_0)^{4/3} t^{2/3} k^{-5/3}, \quad (29)$$

$$S_p^T(r) = \langle [T(\mathbf{r}, t) - T(\mathbf{0}, t)]^p \rangle \simeq \theta_0^p (\beta g \theta_0)^{-p/3} t^{-2p/3} r^{p/3}, \quad (30)$$

$$E_T(k) \simeq \theta_0^2 (\beta g \theta_0)^{-2/3} t^{-4/3} k^{-5/3}, \quad (31)$$

whereas for the 2D case

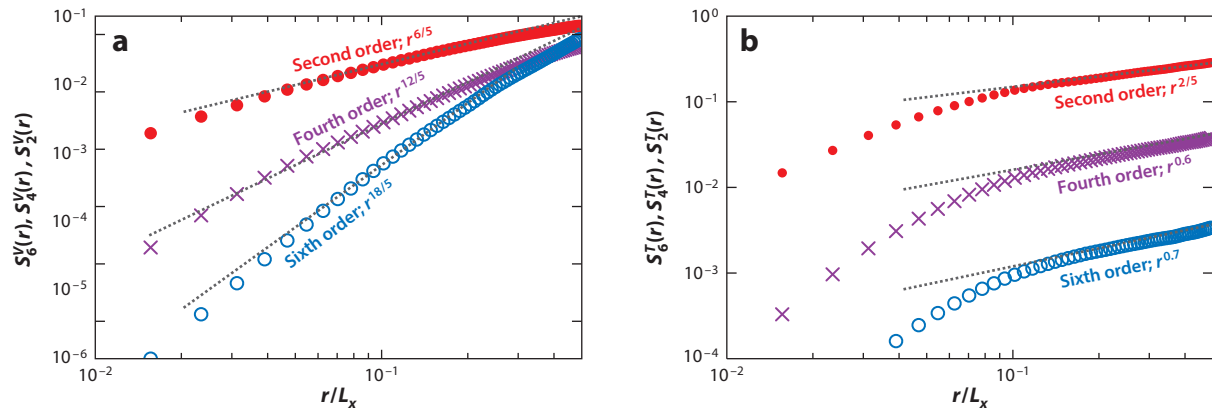
$$S_p(r) = \left\langle \left[ (\mathbf{u}(\mathbf{r}, t) - \mathbf{u}(\mathbf{0}, t)) \cdot \frac{\mathbf{r}}{r} \right]^p \right\rangle \simeq (\beta g \theta_0)^{2p/5} t^{-p/5} r^{3p/5}, \quad (32)$$

$$E(k) \simeq (\beta g \theta_0)^{4/5} t^{-2/5} k^{-11/5}, \quad (33)$$

$$S_p^T(r) = \langle [T(\mathbf{r}, t) - T(\mathbf{0}, t)]^p \rangle \simeq \theta_0^p (\beta g \theta_0)^{-p/5} t^{-2p/5} r^{p/5}, \quad (34)$$

$$E_T(k) \simeq \theta_0^2 (\beta g \theta_0)^{-2/5} t^{-4/5} k^{-7/5}. \quad (35)$$

In the above expressions, brackets denote space averages within the mixing layer under the hypothesis of small-scale homogeneity and isotropy. Homogeneity actually follows from the observation that the horizontally ensemble-averaged temperature field,  $\overline{T}(z)$ , behaves linearly along the gravitational direction (see Section 3) and that the equation for the horizontally ensemble-averaged velocity reduces to  $\partial \overline{p}(z)/\partial z = \beta g \overline{T}(z)$ . From these two remarks, it immediately follows that temperature fluctuations around  $\overline{T}(z)$  are homogeneous, and the same is true for the velocity: This is indeed forced by temperature fluctuations, with the horizontally averaged temperature balanced by the averaged pressure field, as stated above. The above scenario is confirmed by deep analysis on the distribution of the local dissipation scale carried out in two dimensions by Qiu


**Figure 4**

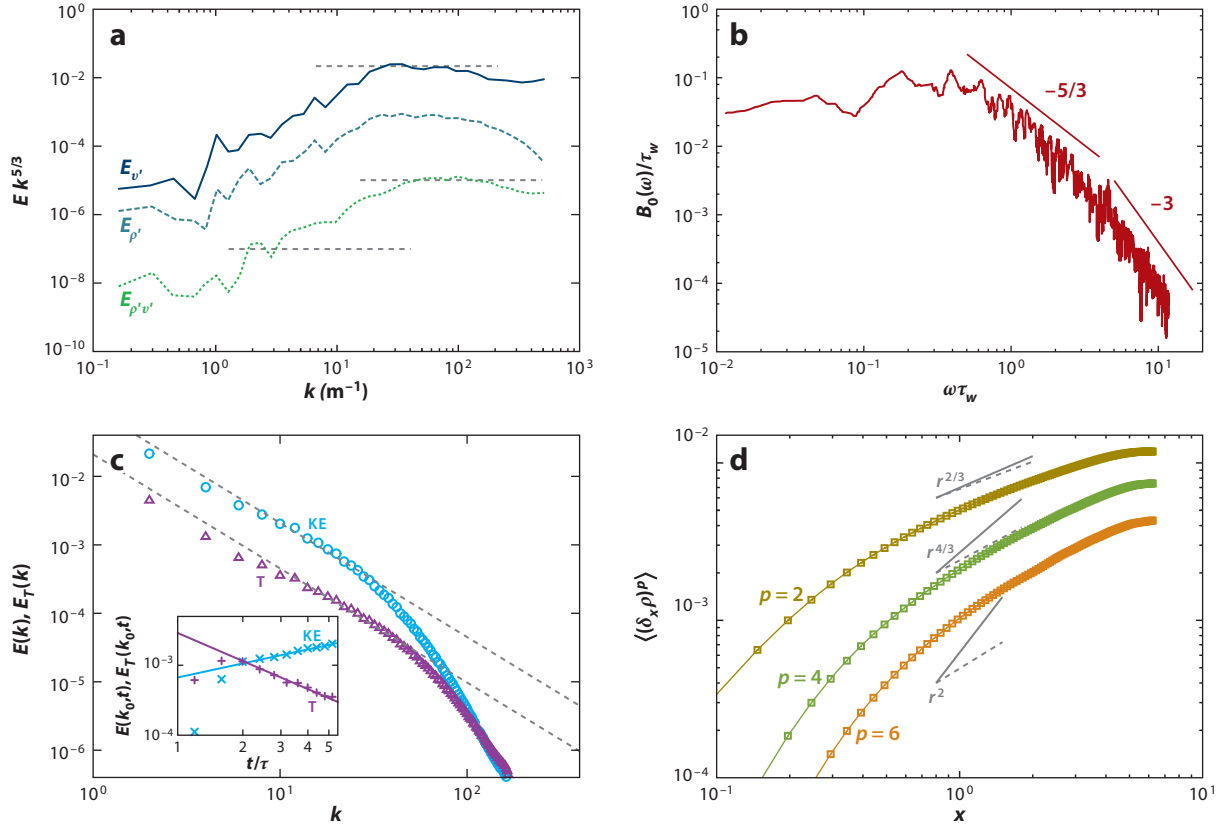
Isotropic moments of the longitudinal (a) velocity differences and (b) temperature differences of orders 2, 4, and 6 obtained by averaging over all directions of separation  $\mathbf{r}$ . In panel a, the gray dashed lines represent the Bolgiano dimensional prediction  $S_p(r) \simeq r^{-3p/5}$ , whereas in panel b they represent the best-fit scaling exponents, which for  $p = 4$  and  $p = 6$  are anomalous. Figure adapted with permission from Celani et al. (2006).

et al. (2014). The tendency toward isotropy restoration of small-scale fluctuations has been numerically verified by Biferale et al. (2010) in two dimensions and Boffetta et al. (2009, 2010d) in three dimensions and experimentally verified by Ramaprabhu & Andrews (2004).

The validity of the BO59 scenario encoded in the scaling relations in Equations 32–35 was first addressed by DNS in two dimensions by Celani et al. (2006), exploiting a standard pseudo-spectral method, and successively by Biferale et al. (2010) using a thermal lattice Boltzmann method. **Figure 4** illustrates the velocity and temperature structure functions of orders  $p = 2$ ,  $p = 4$ , and  $p = 6$  from Celani et al. (2006). The curves for  $p = 2$  closely agree with the Chertkov (2003) theory for both the spatial and temporal scaling. A close look at higher orders reveals the presence of non-negligible deviations with respect to the dimensional predictions. The presence of these intermittency corrections has also been confirmed by Biferale et al. (2010) and Zhou (2013). Intermittency was not observed for the velocity structure functions that exhibit, within error bars, dimensional scaling, as in the case of the inverse cascade in 2D Navier-Stokes turbulence (Boffetta & Ecke 2012).

Interestingly, the scaling exponents for velocity and temperature structure functions obtained by Celani et al. (2006) are in remarkable agreement with those found for the 2D turbulent RB system forced by a mean gradient analyzed by Celani et al. (2002). This supports the universality of scaling exponents in two systems with different boundary conditions. At the level of spectral observables for both velocity and temperature, BO59 scaling, both in space and in time, has received strong support from numerical simulations by Zhou (2013).

With regard to the 3D case, evidence of an energy cascade from large to small length scales with an associated K41 spectrum (for both velocity and density) has been provided by an air-helium gas channel experiment by Banerjee et al. (2010) (see **Figure 5**). Their observation is consistent with previous measurements in a water channel by Ramaprabhu & Andrews (2004) and Mueschke et al. (2006). However, the mixing layer does not have a sufficient range of scales to make a definitive assessment about the spectral behavior. A detailed analysis based on image-processing techniques by Dalziel et al. (1999) provided the internal structure and statistics of the concentration field. Concentration power spectra have been analyzed, and the Obukhov–Corrsin scenario turned out


**Figure 5**

Kinetic energy (KE) and density/temperature (T) variance spectra for different Rayleigh–Taylor turbulent flows. (a) Turbulent kinetic energy spectrum  $E_{v'}$ , density fluctuation spectrum  $E_{\rho'}$ , and correlation spectrum  $E_{\rho'v'}$  from an air–helium gas experiment at Atwood number  $A = 0.03$ . Spectra are compensated with  $k^{-5/3}$  to show the range of Kolmogorov scaling. Panel a adapted with permission from Banerjee et al. (2010). (b) Density fluctuation spectra from a water experiment at small Atwood number and  $Pr = 7$ . Both the inertial ( $-5/3$ ) and the viscous-convective ( $-3$ ) regimes are observed. Panel b adapted from Wilson & Andrews (2002) with the permission of AIP Publishing. (c) Kinetic energy and temperature (density) variance from direct numerical simulations of the Boussinesq equations. The dashed lines represent Kolmogorov scaling. The inset displays the time evolution of the kinetic energy (blue crosses) and temperature (red plus signs) spectra compared with the dimensional predictions  $t^{2/3}$  and  $t^{-4/3}$ , respectively. Panel c adapted with permission from Boffetta et al. (2009). (d) Density (temperature) structure functions from direct numerical simulations of the Boussinesq equations. The solid lines represent the dimensional Kolmogorov predictions  $S_p^T(r) \simeq r^{p/3}$ , and dashed lines represent the anomalous exponents of a passive scalar with mean scalar gradient (Watanabe & Gotoh 2006). Panel d adapted with permission from Matsumoto (2009).

to be compatible with the experimental observations. A similar conclusion was drawn by Wilson & Andrews (2002) (Figure 5).

The K41 scenario was also confirmed in high-resolution numerical simulations (e.g., Young et al. 2001, Dimonte et al. 2004, Cabot & Cook 2006). Vladimirova & Chertkov (2009) stated that the range of scales compatible with Kolmogorov scaling grows with time and that the viscous scale decreases with time in accordance with predictions by Chertkov (2003). A clear  $k^{-5/3}$  power law has also been extracted for the vertical velocity spectrum and for the density obtained from accurate large-eddy simulations by Cook et al. (2004).

The advantage of numerical strategies with respect to experiments is that information on the intermittency corrections becomes available (e.g., Matsumoto 2009, Boffetta et al. 2009, 2010d) (see **Figure 5**). Boffetta et al. (2009, 2010d) showed that the scaling exponents of isotropic longitudinal velocity structure functions are indistinguishable from those of Navier-Stokes turbulence at comparable Reynolds numbers (see, e.g., Warhaft 2000, Watanabe & Gotoh 2004), supporting the universality of turbulence with respect to the forcing mechanism. Antonelli et al. (2007) drew a similar conclusion for buoyancy-dominated turbulent flows in the atmospheric convective boundary layer.

## 4.2. Bolgiano Scaling and Bolgiano Length

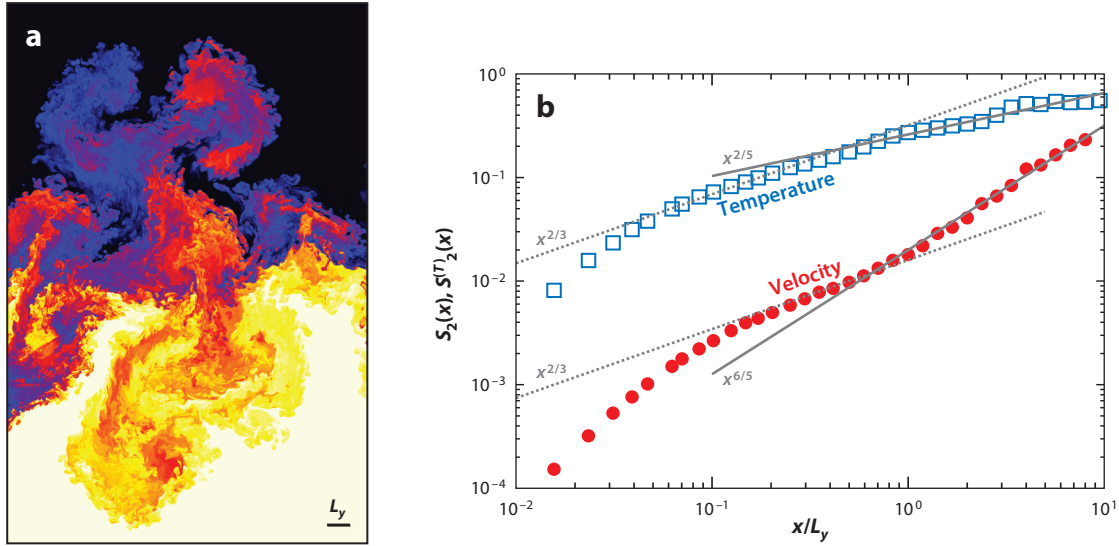
As discussed in Section 4, according to the theory of Chertkov (2003), the Bolgiano scale  $L_B = \varepsilon^{5/4} \varepsilon_T^{-3/4} (\beta g)^{-3/2}$  (above which the buoyancy forces overcome the inertial forces) coincides with the integral scales,  $L_B \simeq b$ , in three dimensions, whereas it is the smallest active scale,  $L_B \simeq \eta$ , in two dimensions. Therefore, the inertial range of scales  $\eta \ll r \ll b$  displays K41 scaling in three dimensions and BO59 scaling in two dimensions, and the Bolgiano scale does not explicitly appear in the range of active scales. The identification of the Bolgiano scale, and of the associated BO59 scaling, is one of the open problems in the study of turbulent convection, in particular for RB convection (Lohse & Xia 2010).

Boffetta et al. (2012a) proposed that the Bolgiano scale could emerge in the inertial range by considering a configuration intermediate between two and three dimensions. They verified this simple idea using high-resolution DNS of a geometrically confined turbulent RT system with one side,  $L_y$ , much smaller than the other two,  $L_x$  and  $L_z$ . At small times, when  $b(t) \ll L_y$ , the dynamics is purely 3D. When the mixing layer length becomes larger than  $L_y$ , the system is effectively 2D at large scale. The scale  $L_y$  is thus expected to be the Bolgiano length of the system, at which a transition from K41 to BO59 occurs. **Figure 6a** shows a vertical section ( $x$ - $z$ ) of the temperature field in which large-scale 2D structures coexist with small-scale 3D turbulence. The presence of two different scaling regimes is displayed in **Figure 6b**, which shows structure functions for both velocity and temperature fluctuations. The crossover between the two scalings appears at  $L_y$ , which is therefore identified as the Bolgiano scale of the system.

We conclude this section by recalling that the effects of geometrical confinement in RT turbulence can be even more dramatic when two dimensions are confined (in a quasi-1D geometry). In this case, large-scale quantities are also affected by the confinement: For example, the width of the mixing layer  $b(t)$  displays anomalous, subdiffusive growth, as observed experimentally by Dalziel et al. (2008) and numerically by Lawrie & Dalziel (2011) and Boffetta et al. (2012c).

## 5. VISCOELASTIC RAYLEIGH-TAYLOR TURBULENCE

Polymer additives produce dramatic effects on turbulent flows, the most important being the reduction of turbulent drag up to 80% when a few parts per million of long-chain polymers are added to water (Virk 1975). The natural framework of drag-reduction studies is the case of pipe flow or channel flow: Within this context, the reduction of frictional drag manifests as an increase of the mean flow across the pipe or channel at a given pressure drop. In turbulent convection, together with mass, heat is also transported by the flow; therefore, an intriguing question is whether turbulent heat transport is also affected and, in particular, if it can be enhanced by the presence of polymers. This issue has been addressed only in recent years within the framework of RB turbulent convection. Recent studies have shown that, in the range of  $Ra$  investigated in which the contribution to the dissipation rates from the boundary layers is significant, polymers reduce the


**Figure 6**

(a) Vertical section of the temperature field for a simulation of confined Rayleigh–Taylor turbulence at a resolution of  $4,096 \times 128 \times 8,192$  with an aspect ratio  $L_y/L_x = 1/32$ ,  $L_z/L_x = 2$ . Quasi-2D plumes are evident at large scales, together with small-scale 3D fluctuations. The small black bar represents the dimension  $L_y$  of the confining layer shown in panel a. (b) Second-order velocity and temperature structure functions computed in the central part of the mixing layer shown in panel a. Dotted lines represent Kolmogorov scaling  $x^{2/3}$  expected for small-scale (below  $L_y$ ) fluctuations. Solid lines show Bolgiano scaling  $x^{6/5}$  and  $x^{2/5}$  (for velocity and temperature structure functions, respectively) predicted for scales  $x > L_y$ .

global heat transport by a small amount, as found in experiments by Ahlers & Nikolaenko (2010). An enhancement of the heat transport has been observed locally by Xie et al. (2015) within the bulk region of turbulent thermal convection, where the effects of boundary layers are negligible, and also in numerical simulations by Benzi et al. (2010) of homogeneous convection, in which boundaries were removed. It is therefore natural to investigate if and how polymer additives affect the dynamics of RT turbulence. Indeed, the development of the mixing layer implies a vertical transport of mass under the effect of gravity, which has analogies with transport in a channel under pressure forces. Moreover, the absence of boundary layers in the development of RT turbulence suggests that the effects of polymer additives can be very different with respect to the case of RB convection.

Theoretical studies of polymer additives in turbulence are usually based on viscoelastic models in which polymer effects are embodied in a positive symmetric conformation tensor  $\sigma(\mathbf{x}, t) = \langle \mathbf{RR} \rangle / R_0^2$  representing the local polymer elongation averaged over the thermal noise (and normalized to the equilibrium length  $R_0$ ) (Bird et al. 1977). One of the simplest viscoelastic models is the linear Oldroyd-B model, which, for the OB framework, reads

$$\begin{aligned} \partial_t \mathbf{u} + \mathbf{u} \cdot \nabla \mathbf{u} &= -\nabla p + \nu \nabla^2 \mathbf{u} - \beta \mathbf{g} T + \frac{2\nu\gamma}{\tau_p} \nabla \cdot \sigma, \\ \partial_t T + \mathbf{u} \cdot \nabla T &= \kappa \nabla^2 T, \\ \partial_t \sigma + \mathbf{u} \cdot \nabla \sigma &= (\nabla \mathbf{u})^T \cdot \sigma + \sigma \cdot (\nabla \mathbf{u}) - \frac{2}{\tau_p} (\sigma - \mathbb{I}) + \kappa_p \nabla^2 \sigma. \end{aligned} \quad (36)$$

In Equation 36,  $\gamma$  is the zero-shear polymer contribution to the total viscosity  $\nu_T = \nu(1 + \gamma)$  (which is proportional to the polymer concentration),  $\tau_p$  is the (longest) polymer relaxation time [i.e., the Zimm relaxation time for a linear chain (Bird et al. 1977)], and  $\kappa_p$  represents a polymer

diffusivity needed to prevent numerical instabilities (Sureshkumar & Beris 1995). When the fluid is at rest, the polymer conformation tensor relaxes to the equilibrium configuration  $\sigma = \mathbb{I}$ , which is therefore the initial condition at  $t = 0$ . As turbulence develops in the mixing layer, polymers are stretched and produce an elastic stress on the flow proportional to  $\nabla \cdot \sigma$ .

The presence of polymers changes the energy balance with respect to the Newtonian fluid. The total energy has an additional elastic contribution  $\Sigma = (\nu\gamma)/(\tau_p)[(tr\sigma) - 3]$ , and this changes Equation 15 to

$$\kappa \frac{\beta g \theta_0}{b} Nu = \frac{dE}{dt} + \frac{d\Sigma}{dt} + \varepsilon_v + \varepsilon_\Sigma, \quad (37)$$

where  $\varepsilon_\Sigma = 2\Sigma/\tau_p$  is the elastic dissipation.

A first indication of the effects of the polymer solution in the development of RT turbulence is provided by linear stability analysis of the viscoelastic RT model (Equation 36). Boffetta et al. (2010c) demonstrated that the polymer solution speeds up the linear phase of the RT instability by a factor that increases with the elasticity of the solution (proportional to  $\tau_p$ ). This phenomenon is reminiscent of polymer drag reduction in pipe flow.

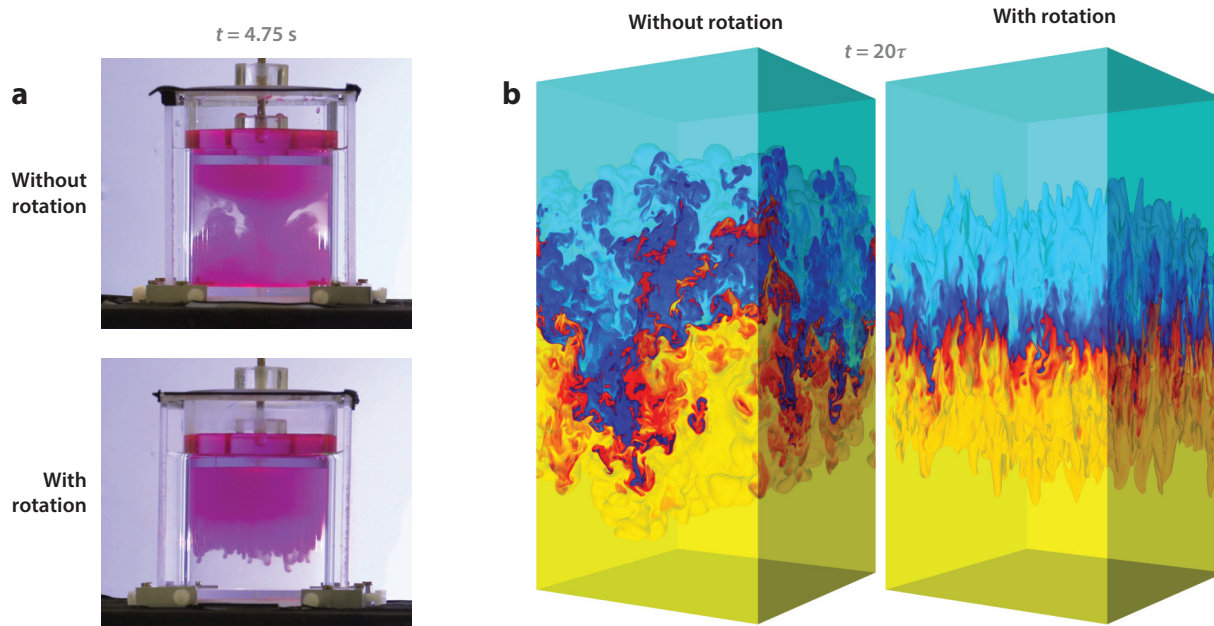
For the nonlinear phase, we assume that turbulence initially follows the 3D K41 scenario described in Section 4.1. The viscous timescale (Equation 23) decreases as  $\tau_\eta \simeq (\beta g \theta_0)^{-1} \nu^{1/2} t^{-1/2}$ ; therefore, the Weissenberg number  $Wi \equiv \tau_p/\tau_\eta$ , a measure of the relative strength of stretching due to velocity gradients and polymer relaxation, thus grows as  $Wi \simeq t^{1/2}$ . Therefore, even in the presence of a very small polymer relaxation time  $\tau_p$ , a coil-stretch transition by which polymers become active is thus expected for sufficiently long evolution times.

With regard to the 2D case, the initial dynamics is ruled by BO scaling according to which the viscous timescale is now given by Equation 27:  $\tau_\eta \simeq (\beta g \theta_0)^{-1/2} \nu^{1/4} t^{1/4}$ . Therefore, the Weissenberg number decreases in time as  $Wi \simeq t^{-1/4}$ , and polymers will eventually recover (or remain in) the coiled state.

On the basis of the above dimensional arguments, one may conjecture that viscoelastic effects in three dimensions become increasingly relevant as the system evolves. The opposite conclusion can be drawn in two dimensions, in which the role played by polymers is expected to be transient and to disappear in the late stage of the evolution.

The effect of polymers in RT turbulence has been studied by Boffetta et al. (2010b, 2011) with DNS of the viscoelastic model (Equation 36). As a result of these papers, it has been shown that the mixing layer growth is faster in the viscoelastic case than in the Newtonian case. Polymers thus make the transfer of mass more efficient, which implies that large-scale mixing is enhanced. The opposite happens for small-scale mixing: Temperature variance has been found to be larger in the viscoelastic case than in the Newtonian case. Thermal plumes are thus more coherent in the viscoelastic case, which is expected to contribute to the enhancement of heat transfer with respect to the Newtonian case. The temperature variance indeed enters into the definition of the Nusselt number (see Section 3.2). It turns out that polymers increase the values attained by  $Nu$  and  $Ra$  at late times. The ultimate-state scaling  $Nu \simeq Ra^{1/2}$  has been observed in both the Newtonian and viscoelastic cases.

The polymer heat transfer enhancement in RT turbulence can be interpreted in terms of polymer drag reduction between rising and sinking plumes. For the RT turbulent system, Boffetta et al. (2011) proposed a quantitative definition of drag in terms of the dimensionless coefficient  $\alpha$  (see Section 3). The increase of  $\alpha$  induced by polymers observed by Boffetta et al. (2010b, 2011) has been interpreted as a reduction of the turbulent drag, as the RT viscoelastic system is able to more efficiently convert potential energy into kinetic energy contained in large plumes. Conversely, the turbulent transfer of kinetic energy toward small scales is reduced, thus reducing the viscous dissipation. With respect to Newtonian turbulence, a suppression of small-scale velocity


**Figure 7**

Rotating Rayleigh–Taylor turbulence. (a) The evolution of the Rayleigh–Taylor instability in a paramagnetic liquid (*pink*) overlying a diamagnetic liquid (*clear*) without rotation (*upper image*) and with  $\Omega = 4.6$  rad s<sup>-1</sup> (*lower image*). Magnetic body forces are used to destabilize the gravitationally stable system. Panel *a* reproduced with permission from Baldwin et al. (2015). (b) The temperature field, at the same time  $t = 20\tau$ , for two simulations of the Oberbeck–Boussinesq equations with the Coriolis force starting from the same initial condition, with  $\Omega = 0$  (*left*) and with  $\Omega\tau = 20$  (*right*) [ $\tau = (L_z/Ag)^{1/2}$ ].

fluctuations is observed, accompanied by an increase in the kinetic energy of the large-scale velocity components. This is the phenomenology of polymer drag reduction observed in homogeneous, isotropic turbulence (see, e.g., De Angelis et al. 2005).

## 6. RAYLEIGH–TAYLOR TURBULENCE IN THE PRESENCE OF ROTATION

It is well established that the Coriolis force in rotating fluids can reduce the instability of a flow. The effect of rotation on RT instability was first considered by Chandrasekhar (1961), who concluded that it slows down the instability, and was later extended by Tao et al. (2013) to the nonlinear stage. These predictions have been confirmed in numerical simulations by Carnevale et al. (2002) and more recently in experiments by Baldwin et al. (2015).

The effect of rotation on the turbulent phase is less clear. In the case of RB convection, turbulence can increase the vertical heat transfer at moderate rotation (and Rayleigh number) by enhancing the Ekman pumping of temperature from the boundaries. For stronger rotation, the bidimensionalization of the flow by the Taylor–Proudman effect (Tritton 1988) reduces the vertical flow and heat transfer. As RT turbulence has no boundary layers, we expect that here rotation monotonically suppresses the vertical transfer of heat.

The effect of rotation on RT turbulence can be studied in the OB framework by adding the Coriolis force  $2\Omega \times \mathbf{u}$  [with  $\Omega = (0, 0, \Omega)$ ] to Equation 2. The dimensionless Rossby number  $Ro = U/(2\Omega b)$ , which measures the relative strength of the inertial forces to the Coriolis force,

here is found to decrease, using Equations 7 and 8, as  $Ro \simeq 1/(\Omega t)$ . Therefore, the effect of rotation, even if negligible at the initial time, becomes more important and competes with the inertial, and buoyancy, forces for  $t \gtrsim 1/\Omega$ . **Figure 7** shows that the effect of rotation is already evident at a qualitative level with the deformation of the thermal plumes, which become elongated as a manifestation of the Taylor-Proudman theorem. The suppression of vertical fluctuations causes a reduction in the growth of the mixing layer, which is found to be monotonic in  $\Omega$ . Therefore, from the discussion in Section 3.2, the evolution of both  $Ra$  and  $Nu$  (proportional to  $b^3$  and  $b$ , respectively) is slowed down by rotation. Moreover, the turbulent heat transfer is also reduced by rotation at a given  $Ra$ : As a consequence of the suppression of the vertical fluctuations, the correlation  $\langle wT \rangle$  is reduced with respect to the nonrotating case.

## 7. REACTIVE RAYLEIGH-TAYLOR TURBULENCE

Recently, there has been an increasing interest in reactive RT turbulence, which finds applications in several natural phenomena and technologies, as discussed in Section 1. Briefly, we only address here the general question of how reaction affects the phenomenology of RT turbulence, in particular, the competition between gravitational forces, which mixes the two fluids and produces a mixing layer with uniform temperature, and combustion, which produces a propagating front that works against mixing.

Vladimirova & Rosner (2003) studied the effect of turbulence on the speed of a front propagating vertically against gravity by 2D simulations in an elongated domain. Chertkov et al. (2009) extended these simulations to an unconfined domain (with periodic boundary conditions) with an FKPP reaction model (Fisher 1937) characterized by a reaction time  $\tau_r$ , whereas Hicks (2015) used a different reaction that was linearly stable at the ignition temperature. The peculiarity of RT turbulence, with respect to other examples of turbulent combustion, is that the ratio of the

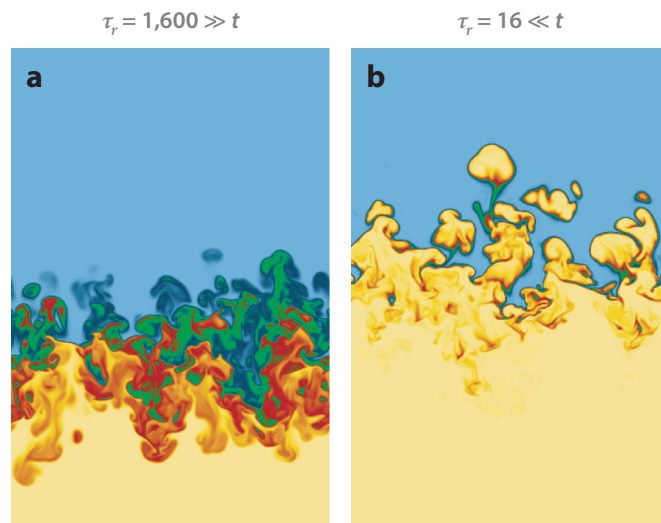


**Figure 8**

Reactive Rayleigh–Taylor turbulence, showing vertical sections of the temperature field at time  $t = 128$  for two 3D simulations of Rayleigh–Taylor turbulence with different reaction times: (a)  $\tau_r = 1,600 \gg t$  and (b)  $\tau_r = 16 \ll t$ . There is a vertical shift of the mixing layer due to the propagation of the reaction. Images courtesy of N. Vladimirova.

turbulent mixing time  $T$  to the reaction time (the so-called Damköler number,  $Da = T/\tau_r$ ) grows linearly in time as  $T \simeq b(t)/U(t) \simeq t$ . Therefore, even in the case of a slow reaction, the system will undergo a transition to the fast reaction regime  $Da > 1$  in which a new segregated stage appears. In this new regime, the mixing layer is characterized by the presence of a pure phase, shown in **Figure 8**, as the turbulent temperature fluctuations have been eliminated by combustion and separated by a thin active interface. Similar results have been obtained by Biferale et al. (2011a) and Hicks & Rosner (2010) for the 2D case. One interesting result of these investigations is that, despite the strong effects on the distribution of the temperature field (which is already evident from **Figure 8**), the amplitude and speed of the mixing layer are weakly affected by the reaction. The main effect in the fast reaction regime is a vertical drift of the mixing layer due to the propagation of the front.

### SUMMARY POINTS

1. The development of a direct cascade of energy in the mixing layer with the Kolmogorov–Obukhov spectrum is well established by experiments and numerical simulations.
2. In two dimensions, numerical simulations and theoretical arguments support the presence of an inverse cascade of energy with Bolgiano–Obukhov scaling, with temperature fluctuations injecting energy at all scales.
3. RT turbulence undergoes a transition from a 3D to 2D phenomenology when the width of the mixing layer becomes larger than the scale of confinement. This latter scale is identified with the Bolgiano scale.
4. Heat transfer in RT turbulence displays the ultimate state scaling of thermal convection, thus highlighting the relationship between the absence of boundary layers and the emergence of the ultimate state scaling, in both two and three dimensions.
5. Heat transfer in RT convection can be enhanced via polymer additives. This phenomenon is accompanied by a speedup of mixing layer growth.

### FUTURE ISSUES

1. A challenge for future experiments is to measure small-scale velocity and temperature fluctuations, in both 2D and 3D configurations, and to identify the Bolgiano scale in confined experiments.
2. Experiments in viscoelastic RT mixing should confirm the enhancement of heat transfer observed in simulations and clarify the differences between RT and RB phenomenology in this respect.
3. A better understanding of the effect of rotation on RT turbulence is important for astrophysical applications.
4. We need a better understanding of the role of surface tension for immiscible RT turbulence with the verification of theoretical predictions.
5. Theoretical, numerical, and experimental studies are required for RT turbulence and mixing of complex particles.

## DISCLOSURE STATEMENT

The authors are not aware of any biases that might be perceived as affecting the objectivity of this review.

## ACKNOWLEDGMENTS

The authors thank Luca Biferale, Alessandro Bottaro, Antonio Celani, Filippo De Lillo, Stefano Musacchio, and Lara Vozella for fruitful collaborations and extensive discussions about Rayleigh–Taylor turbulence. They acknowledge Arindam Banerjee for several suggestions on the manuscript. The authors also thank Malcolm Andrews, Andrew Cook, Richard Hill, Takeshi Matsumoto, Petros Tzeferacos, and Natalia Vladimirova for help with the figures. A. Mazzino acknowledges financial support from PRIN 2012 (project D38C13000610001 funded by the Italian Ministry of Education) and the Italian flagship project RITMARE.

## LITERATURE CITED

- Abarzhi S. 2010a. On fundamentals of Rayleigh–Taylor turbulent mixing. *Europhys. Lett.* 91:35001
- Abarzhi S. 2010b. Review of theoretical modelling approaches of Rayleigh–Taylor instabilities and turbulent mixing. *Philos. Trans. R. Soc. Lond. A* 368:1809–28
- Agee E. 1975. Some inferences of eddy viscosity associated with instabilities in the atmosphere. *J. Atmos. Sci.* 32:642–46
- Ahlers G, Grossmann S, Lohse D. 2009. Heat transfer and large scale dynamics in turbulent Rayleigh–Bénard convection. *Rev. Mod. Phys.* 81:503–37
- Ahlers G, Nikolaenko A. 2010. Effect of a polymer additive on heat transport in turbulent Rayleigh–Bénard convection. *Phys. Rev. Lett.* 104:034503
- Andrews M, Dalziel S. 2010. Small Atwood number Rayleigh–Taylor experiments. *Philos. Trans. R. Soc. A* 368:1663–79
- Andrews M, Spalding D. 1990. A simple experiment to investigate two-dimensional mixing by Rayleigh–Taylor instability. *Phys. Fluids A* 2:922–27
- Antonelli M, Lanotte A, Mazzino A. 2007. Anisotropies and universality of buoyancy-dominated turbulent fluctuations: a large-eddy simulation study. *J. Atmos. Sci.* 64:2642–56
- Baldwin K, Scase M, Hill R. 2015. The inhibition of the Rayleigh–Taylor instability by rotation. *Sci. Rep.* 5:11706
- Banerjee A, Andrews M. 2006. Statistically steady measurements of Rayleigh–Taylor mixing in a gas channel. *Phys. Fluids* 18:035107
- Banerjee A, Andrews M. 2009. 3D simulations to investigate initial condition effects on the growth of Rayleigh–Taylor mixing. *Int. J. Heat Mass Transf.* 52:3906–17
- Banerjee A, Kraft W, Andrews M. 2010. Detailed measurements of a statistically steady Rayleigh–Taylor mixing layer from small to high Atwood numbers. *J. Fluid Mech.* 659:127–90
- Bell J, Day M, Rendleman C, Woosley S, Zingale M. 2004. Direct numerical simulations of type Ia supernovae flames. II. The Rayleigh–Taylor instability. *Astrophys. J.* 608:883–906
- Bellman R, Pennington R. 1954. Effects of surface tension and viscosity on Taylor instability. *Phys. Rev. Lett.* 12:151–62
- Benzi R, Ching E, De Angelis E. 2010. Effect of polymer additives on heat transport in turbulent thermal convection. *Phys. Rev. Lett.* 104:024502
- Biferale L, Mantovani F, Sbragaglia M, Scagliarini A, Toschi F, Tripiccione R. 2010. High resolution numerical study of Rayleigh–Taylor turbulence using a thermal lattice Boltzmann scheme. *Phys. Fluids* 22:115112
- Biferale L, Mantovani F, Sbragaglia M, Scagliarini A, Toschi F, Tripiccione R. 2011a. Reactive Rayleigh–Taylor systems: front propagation and non-stationarity. *Europhys. Lett.* 94:54004
- Biferale L, Mantovani F, Sbragaglia M, Scagliarini A, Toschi F, Tripiccione R. 2011b. Second-order closure in stratified turbulence: simulations and modeling of bulk and entrainment regions. *Phys. Rev. E* 84:016305

- Bird R, Armstrong R, Hassager O, Curtiss C. 1977. *Dynamics of Polymeric Liquids*, Vol. 1. New York: Wiley
- Bodenschatz E, Pesch W, Ahlers G. 2000. Recent developments in Rayleigh-Bénard convection. *Annu. Rev. Fluid Mech.* 32:709–78
- Boffetta G, De Lillo F, Mazzino A, Musacchio S. 2012a. Bolgiano scale in confined Rayleigh-Taylor turbulence. *J. Fluid Mech.* 690:426–40
- Boffetta G, De Lillo F, Mazzino A, Vozella L. 2012b. The ultimate state of thermal convection in Rayleigh-Taylor turbulence. *Physica D* 241:137–40
- Boffetta G, De Lillo F, Musacchio S. 2010a. Nonlinear diffusion model for Rayleigh-Taylor mixing. *Phys. Rev. Lett.* 104:034505
- Boffetta G, De Lillo F, Musacchio S. 2012c. Anomalous diffusion in confined turbulent convection. *Phys. Rev. E* 85:066322
- Boffetta G, Ecke R. 2012. Two-dimensional turbulence. *Annu. Rev. Fluid Mech.* 44:427–51
- Boffetta G, Mazzino A, Musacchio S. 2011. Effects of polymer additives on Rayleigh-Taylor turbulence. *Phys. Rev. E* 83:056318
- Boffetta G, Mazzino A, Musacchio S, Vozella L. 2009. Kolmogorov scaling and intermittency in Rayleigh-Taylor turbulence. *Phys. Rev. E* 79:065301
- Boffetta G, Mazzino A, Musacchio S, Vozella L. 2010b. Polymer heat transport enhancement in thermal convection: the case of Rayleigh-Taylor turbulence. *Phys. Rev. Lett.* 104:184501
- Boffetta G, Mazzino A, Musacchio S, Vozella L. 2010c. Rayleigh-Taylor instability in a viscoelastic binary fluid. *J. Fluid Mech.* 643:127–36
- Boffetta G, Mazzino A, Musacchio S, Vozella L. 2010d. Statistics of mixing in three-dimensional Rayleigh-Taylor turbulence at low Atwood number and Prandtl number one. *Phys. Fluids* 22:035109
- Bolgiano R. 1959. Turbulent spectra in a stably stratified atmosphere. *J. Geophys. Res.* 64:2226–29
- Cabot W, Cook A. 2006. Reynolds number effects on Rayleigh-Taylor instability with possible implications for type Ia supernovae. *Nat. Phys.* 2:562–68
- Canuto V, Goldman I. 1985. Analytical model for large-scale turbulence. *Phys. Rev. Lett.* 54:430–33
- Carnevale G, Orlandi P, Zhou Y, Kloosterziel R. 2002. Rotational suppression of Rayleigh-Taylor instability. *J. Fluid Mech.* 457:181–90
- Celani A, Matsumoto T, Mazzino A, Vergassola M. 2002. Scaling and universality in turbulent convection. *Phys. Rev. Lett.* 88:054503
- Celani A, Mazzino A, Muratore-Ginanneschi P, Vozella L. 2009. Phase-field model for the Rayleigh-Taylor instability of immiscible fluids. *J. Fluid Mech.* 622:115–34
- Celani A, Mazzino A, Vozella L. 2006. Rayleigh-Taylor turbulence in two dimensions. *Phys. Rev. Lett.* 96:134504
- Chandrasekhar S. 1961. *Hydrodynamics and Hydromagnetic Stability*. New York: Oxford Univ. Press
- Chang C. 1959. Dynamic instability of accelerated fluids. *Phys. Fluids* 2:656–63
- Chertkov M. 2003. Phenomenology of Rayleigh-Taylor turbulence. *Phys. Rev. Lett.* 91:115001
- Chertkov M, Kolokolov I, Lebedev V. 2005. Effects of surface tension on immiscible Rayleigh-Taylor turbulence. *Phys. Rev. E* 71:055301
- Chertkov M, Lebedev V, Vladimirova N. 2009. Reactive Rayleigh-Taylor turbulence. *J. Fluid Mech.* 633:1–16
- Cholemani M, Arakeri J. 2009. Axially homogeneous, zero mean flow buoyancy-driven turbulence in a vertical pipe. *J. Fluid Mech.* 621:69–102
- Cook A, Cabot W, Miller P. 2004. The mixing transition in Rayleigh-Taylor instability. *J. Fluid Mech.* 511:333–62
- Corrsin S. 1951. On the spectrum of isotropic temperature fluctuations in an isotropic turbulence. *J. Appl. Phys.* 22:469–73
- Dalziel S. 1993. Rayleigh-Taylor instability: experiments with image analysis. *Dyn. Atmos. Oceans* 20:127–53
- Dalziel S, Linden P, Youngs D. 1999. Self-similarity and internal structure of turbulence induced by Rayleigh-Taylor instability. *J. Fluid Mech.* 399:1–48
- Dalziel S, Patterson M, Caulfield C, Coomaraswamy I. 2008. Mixing efficiency in high-aspect-ratio Rayleigh-Taylor experiments. *Phys. Fluids* 20:065106
- De Angelis E, Casciola C, Benzi R, Piva R. 2005. Homogeneous isotropic turbulence in dilute polymers. *J. Fluid Mech.* 531:1–10

- Dimonte G, Schneider M. 1996. Turbulent Rayleigh–Taylor instability experiments with variable acceleration. *Phys. Rev. E* 54:3740–43
- Dimonte G, Youngs D, Dimits A, Weber S, Marinak M, et al. 2004. A comparative study of the turbulent Rayleigh–Taylor instability using high-resolution three-dimensional numerical simulations: the Alpha-Group collaboration. *Phys. Fluids* 16:1668–93
- Drazin P, Reid W. 1981. *Hydrodynamic Stability*. Cambridge, UK: Cambridge Univ. Press
- Duff R, Harlow F, Hirt C. 1962. Effects of diffusion on interface instability between gases. *Phys. Fluids* 5:417–25
- Fermi E, von Neumann J. 1955. *Taylor instability of incompressible liquids*. Rep. AECU2979, Los Alamos Sci. Lab., Los Alamos, NM
- Fisher R. 1937. The wave of advance of advantageous genes. *Ann. Eugen.* 7:355–69
- Frisch U. 1995. *Turbulence: The Legacy of A.N. Kolmogorov*. Cambridge, UK: Cambridge Univ. Press
- Funfschilling D, Bodenschatz E, Ahlers G. 2009. Search for the ultimate state in turbulent Rayleigh–Bénard convection. *Phys. Rev. Lett.* 103:014503
- Garabedian P. 1957. On steady-state bubbles generated by Taylor instability. *Proc. R. Soc. Lond. A* 241:423–31
- Gibert M, Pabiou H, Chilla F, Castaing B. 2006. High-Rayleigh-number convection in a vertical channel. *Phys. Rev. Lett.* 96:084501
- Goncharov V. 2002. Analytical model of nonlinear, single-mode, classical Rayleigh–Taylor instability at arbitrary Atwood numbers. *Phys. Rev. Lett.* 88:134502
- Grossmann S, Lohse D. 2000. Scaling in thermal convection: a unifying theory. *J. Fluid Mech.* 407:27–56
- Hecht J, Alon U, Shvarts D. 1994. Potential flow models of Rayleigh–Taylor and Richtmyer–Meshkov bubble fronts. *Phys. Fluids* 6:4019–30
- Hicks E. 2015. Rayleigh–Taylor unstable flames—fast or faster? *Astrophys. J.* 803:72
- Hicks E, Rosner R. 2010. Effects of burning on the development of 2D turbulence. *Physica Scr.* 142:014046
- Hillebrandt W, Niemeyer J. 2000. Type Ia supernova explosion models. *Annu. Rev. Astron. Astrophys.* 38:191–230
- Huang Z, De Luca A, Atherton T, Bird M, Rosenblatt C, Carlès P. 2007. Rayleigh–Taylor instability experiments with precise and arbitrary control of the initial interface shape. *Phys. Rev. Lett.* 99:204502
- Kilkenny J, Glendinning S, Haan S, Hammel B, Lindl J, et al. 1994. A review of the ablative stabilization of the Rayleigh–Taylor instability in regimes relevant to inertial confinement fusion. *Phys. Plasmas* 1:1379–89
- Kolmogorov A. 1941. The local structure of turbulence in incompressible viscous fluid for very large Reynolds numbers. *C.R. Acad. Sci. URSS* 30:301–5
- Kraichnan R. 1962. Turbulent thermal convection at arbitrary Prandtl number. *Phys. Fluids* 5:1374–89
- Kruskal M, Schwarzschild M. 1954. Some instabilities of a completely ionized plasma. *Proc. R. Soc. Lond. A* 223:348–60
- Kull H. 1991. Theory of the Rayleigh–Taylor instability. *Phys. Rep.* 206:197–325
- Lamb H. 1932. *Hydrodynamics*. Cambridge, UK: Cambridge Univ. Press
- Lawrie A, Dalziel S. 2011. Turbulent diffusion in tall tubes. I. Models for Rayleigh–Taylor instability. *Phys. Fluids* 23:085109
- Lewis D. 1950. The instability of liquid surfaces when accelerated in a direction perpendicular to their planes. II. *Proc. R. Soc. Lond. A* 202:81–96
- Linden P, Redondo J, Youngs D. 1994. Molecular mixing in Rayleigh–Taylor instability. *J. Fluid Mech.* 265:97–124
- Livescu D. 2004. Compressibility effects on the Rayleigh–Taylor instability growth between immiscible fluids. *Phys. Fluids* 16:118–27
- Livescu D. 2013. Numerical simulations of two-fluid turbulent mixing at large density ratios and applications to the Rayleigh–Taylor instability. *Philos. Trans. R. Soc. Lond. A* 371:20120185
- Lohse D, Toschi F. 2003. Ultimate state of thermal convection. *Phys. Rev. Lett.* 90:034502
- Lohse D, Xia K. 2010. Small-scale properties of turbulent Rayleigh–Bénard convection. *Annu. Rev. Fluid Mech.* 42:335–64
- Matsumoto T. 2009. Anomalous scaling of three-dimensional Rayleigh–Taylor turbulence. *Phys. Rev. E* 79:055301
- Menikoff R, Mjolsness R, Sharp D, Zemach C. 1977. Unstable normal mode for Rayleigh–Taylor instability in viscous fluids. *Phys. Fluids* 20:2000–4

- Mikaelian K. 1989. Turbulent mixing generated by Rayleigh-Taylor and Richtmyer-Meshkov instabilities. *Physica D* 36:343–57
- Mikaelian K. 1993. Effect of viscosity on Rayleigh-Taylor and Richtmyer-Meshkov instabilities. *Phys. Rev. E* 47:375–83
- Mitchner M, Landshoff R. 1964. Rayleigh-Taylor instability for compressible fluids. *Phys. Fluids* 7:862–66
- Mueschke N, Andrews M, Schilling O. 2006. Experimental characterization of initial conditions and spatio-temporal evolution of a small-Atwood-number Rayleigh-Taylor mixing layer. *J. Fluid Mech.* 567:27–63
- Neil E, Houseman G. 1999. Rayleigh-Taylor instability of the upper mantle and its role in intraplate orogeny. *Geophys. J. Int.* 138:89–107
- Newcomb W. 1983. Compressibility effect on instability growth rates. *Phys. Fluids* 26:3246
- Niemela J, Skrbek L, Sreenivasan K, Donnelly R. 2000. Turbulent convection at very high Rayleigh numbers. *Nature* 404:837–40
- Obukhov A. 1941. On the distribution of energy in the spectrum of turbulent flow. *C.R. Acad. Sci. URSS* 32:22–24
- Obukhov A. 1949. Temperature field structure in a turbulent flow. *Izv. Acad. Nauk SSSR Geogr. Geophys.* 13:58–69
- Obukhov A. 1959. Effect of Archimedean forces on the structure of the temperature field in a turbulent flow. *Dokl. Akad. Nauk SSSR* 125:1246–49
- Peterson D, Bowers R, Brownell J, Greene A, McLenithan K, et al. 1996. Two-dimensional modeling of magnetically driven Rayleigh-Taylor instabilities in cylindrical Z pinches. *Phys. Plasmas* 3:368–81
- Plesset M. 1954. On the stability of fluid flows with spherical symmetry. *J. Appl. Phys.* 25:96–98
- Poujade O. 2006. Rayleigh-Taylor turbulence is nothing like Kolmogorov turbulence in the self-similar regime. *Phys. Rev. Lett.* 97:185002
- Qiu X, Liu Y, Zhou Q. 2014. Local dissipation scales in two-dimensional Rayleigh-Taylor turbulence. *Phys. Rev. E* 90:043012
- Ramaprabhu P, Andrews M. 2004. Experimental investigation of Rayleigh-Taylor mixing at small Atwood numbers. *J. Fluid Mech.* 502:233–71
- Read K. 1984. Experimental investigation of turbulent mixing by Rayleigh-Taylor instability. *Physica D* 12:45–58
- Ristorcelli J, Clark T. 2004. Rayleigh-Taylor turbulence: self-similar analysis and direct numerical simulations. *J. Fluid Mech.* 507:213–53
- Rivera M, Ecke R. 2007. The Rayleigh-Taylor instability in small aspect ratio containers. *Proc. 10th Int. Workshop Phys. Compressible Turbul. Mixing*, ed. M Legrand, M Vandenboomgaerde, pp. 332–36. Bruyeres-le-Chatel, Fr.: Commis. Energie Atom.
- Sakagami H, Nishihara K. 1990. Three-dimensional Rayleigh-Taylor instability of spherical systems. *Phys. Rev. Lett.* 65:432–35
- Scagliarini A, Biferale L, Sbragaglia M, Sugiyama K, Toschi F. 2010. Lattice Boltzmann methods for thermal flows: continuum limit and applications to compressible Rayleigh-Taylor systems. *Phys. Fluids* 22:055101
- Schneider M, Dimonte G, Remington B. 1998. Large and small scale structure in Rayleigh-Taylor mixing. *Phys. Rev. Lett.* 80:3507–10
- Sharp D. 1984. An overview of Rayleigh-Taylor instability. *Physica D* 12:3–18
- Shultz D, Kanak K, Straka JM, Trapp R, Gordon B, et al. 2006. The mysteries of mammatus clouds: observations and formation mechanisms. *J. Atmos. Sci.* 63:2409–35
- Siggia E. 1994. High Rayleigh number convection. *Annu. Rev. Fluid Mech.* 26:137–68
- Snider D, Andrews M. 1994. Rayleigh-Taylor and shear driven mixing with an unstable thermal stratification. *Phys. Fluids* 6:3324–34
- Soulard O. 2012. Implications of the Monin-Yaglom relation for Rayleigh-Taylor turbulence. *Phys. Rev. Lett.* 109:254501
- Soulard O, Griffond J. 2012. Inertial-range anisotropy in Rayleigh-Taylor turbulence. *Phys. Fluids* 24:025101
- Soulard O, Griffond J, Gréa B. 2015. Large-scale analysis of unconfined self-similar Rayleigh-Taylor turbulence. *Phys. Fluids* 27:095103
- Spiegel E. 1971. Convection in stars: I. Basic Boussinesq convection. *Annu. Rev. Astron. Astrophys.* 9:323–52

- Sreenivasan KR, Abarzhi SI. 2013. Acceleration and turbulence in Rayleigh–Taylor mixing. *Philos. Trans. R. Soc. Lond. A* 371:20130267
- Sreenivasan KR, Antonia R. 1997. The phenomenology of small-scale turbulence. *Annu. Rev. Fluid Mech.* 29:435–72
- Stevens R, Verzicco R, Lohse D. 2010. Radial boundary layer structure and Nusselt number in Rayleigh–Bénard convection. *J. Fluid Mech.* 643:495–507
- Sultan P. 1996. Linear theory and modeling of the Rayleigh–Taylor instability leading to the occurrence of equatorial spread *F. J. Geophys. Res. Space Phys.* 101:26875–91
- Sureshkumar R, Beris A. 1995. Effect of artificial stress diffusivity on the stability of numerical calculations and the flow dynamics of time-dependent viscoelastic flows. *J. Non-Newton. Fluid Mech.* 60:53–80
- Tabak M, Hammer J, Glinsky M, Kruer W, Wilks S, et al. 1994. Ignition and high gain with ultrapowerful lasers. *Phys. Plasmas* 1:1626–34
- Tao J, He X, Ye W, Busse F. 2013. Nonlinear Rayleigh–Taylor instability of rotating inviscid fluids. *Phys. Rev. E* 87:013001
- Tritton D. 1988. *Physical Fluid Dynamics*. Oxford, UK: Clarendon
- Virk P. 1975. Drag reduction fundamentals. *AIChE J.* 21:625–56
- Vladimirova N, Chertkov M. 2009. Self-similarity and universality in Rayleigh–Taylor, Boussinesq turbulence. *Phys. Fluids* 21:015102
- Vladimirova N, Rosner R. 2003. Model flames in the Boussinesq limit: the effects of feedback. *Phys. Rev. E* 67:066305
- Warhaft Z. 2000. Passive scalars in turbulent flows. *Annu. Rev. Fluid Mech.* 32:203–40
- Watanabe T, Gotoh T. 2004. Statistics of a passive scalar in homogeneous turbulence. *N. J. Phys.* 6:40
- Watanabe T, Gotoh T. 2006. Intermittency in passive scalar turbulence under the uniform mean scalar gradient. *Phys. Fluids* 18:058105
- Wei T, Livescu D. 2012. Late-time quadratic growth in single-mode Rayleigh–Taylor instability. *Phys. Rev. E* 86:046405
- Weinberg R, Schmeling H. 1992. Polydiapirs: multiwavelength gravity structures. *J. Struct. Geol.* 14:425–36
- Wilson P, Andrews M. 2002. Spectral measurements of Rayleigh–Taylor mixing at small Atwood number. *Phys. Fluids* 14:938–45
- Xie Y, Huang S, Funfschilling D, Li X, Ni R, Xia K. 2015. Effects of polymer additives in the bulk of turbulent thermal convection. *J. Fluid Mech.* 784:R3
- Young Y, Tufo H, Dubey A, Rosner R. 2001. On the miscible Rayleigh–Taylor instability: two and three dimensions. *J. Fluid Mech.* 447:377–408
- Youngs D. 1991. Three-dimensional numerical simulation of turbulent mixing by Rayleigh–Taylor instability. *Phys. Fluids A* 3:1312–20
- Youngs D. 1992. Experimental investigation of turbulent mixing by Rayleigh–Taylor instability. In *Advances in Compressible Turbulent Mixing*, ed. WP Dannevik, AC Buckingham, CE Leith, pp. 607–26. Washington, DC: US Gov. Print. Off.
- Zhou Q. 2013. Temporal evolution and scaling of mixing in two-dimensional Rayleigh–Taylor turbulence. *Phys. Fluids* 25:085107
- Zhou Y. 2001. A scaling analysis of turbulent flows driven by Rayleigh–Taylor and Richtmyer–Meshkov instabilities. *Phys. Fluids* 13:538–43